Heliyon 10 (2024) e34718

Contents lists available at ScienceDirect

Heliyon

journal homepage: www.cell.com/heliyon

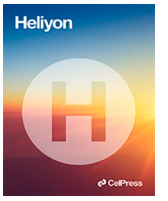

Research article

The Coptidis Rhizoma and Bovis Calculus herb pair attenuates NASH and inhibits the NLRP3 inflammasome activation

Tian Xu [a,b,1], Jiahui Chen [a,1], Qi Shao [a], Jing Ji [a], Qingguo Wang [a], Chongyang Ma [c,*], Xueqian Wang [a,***], Fafeng Cheng [a,**]

[a] School of Traditional Chinese Medicine, Beijing University of Chinese Medicine, Beijing, China
[b] Department of Gastroenterology, Peking Union Medical College Hospital, Peking Union Medical College, Chinese Academy of Medical Sciences, Beijing, China
[c] School of Traditional Chinese Medicine, Capital Medical University, Beijing, China

ARTICLE INFO

Keywords:
NASH
Coptidis rhizoma
Bovis calculus
Herb pair
NLRP3 inflammasome
Network pharmacology

ABSTRACT

The Coptidis Rhizoma and Bovis Calculus herb pair possesses clearing heat and detoxifying effects. The aim of this study was to reveal the effects and mechanisms of the herb pair in the treatment of NASH by network pharmacology and experimental verification. A network pharmacology-based approach was employed to predict the putative mechanism of the herb pair against NASH. The high-fat diet (HFD) and methionine/choline deficient (MCD) diet induced NASH models were used to evaluate efficacy and mechanism of the herb pair. Network pharmacological analysis showed that the herb pair modulated NOD-like receptor pathway. In the HFD mice, herb pair reduced body weight, blood sugar, serum ALT, AST, TBA, TC, TG and LDL-C contents, also improved the general morphology and pathological manifestations. Hepatic transcriptomics study showed that herb pair attenuated NASH by regulating NOD-like receptor signaling pathway. Western blotting showed that herb pair reduced the protein expression levels of NLRP3, cleaved Caspase-1 and cleaved IL-1β. In the MCD mice, herb pair also reduced serum ALT, ALT and TBA levels, improved liver pathological manifestations, inhibited the protein expression levels of NLRP3, cleaved Caspase-1 and cleaved IL-1β. Our findings proved that the Coptidis Rhizoma and Bovis Calculus herb pair attenuates NASH through suppression of NLRP3 inflammasome activation. This will demonstrate effective pharmacological evidence for the clinical application of herb pair.

1. Introduction

Non-alcoholic fatty liver disease (NAFLD) is the most prevalent chronic liver disease globally, affecting approximately 20–25 % of

Abbreviations: Caspase, Cysteinyl aspartate specific proteinase; HDL-C, High density lipoprotein; cholesterolHFD, High fat diet; HP, herb pair; IL-1β, Interleukin-1 beta; MCD, methionine/choline deficient; NAFLD, Non-alcoholic fatty liver disease; NASH, Nonalcoholic steatohepatitis; NLRP3, NOD like receptor thermal protein domain associated protein 3; OGTT, Oral glucose tolerance test; TCM, Traditional Chinese medicine.

* Corresponding author. School of Traditional Chinese Medicine, Capital Medical University, Beijing, 100069, China.
** Corresponding author. School of Traditional Chinese Medicine, Beijing University of Chinese Medicine, Beijing, 100029, China.
*** Corresponding author. School of Traditional Chinese Medicine, Beijing University of Chinese Medicine, Beijing, 100029, China.
E-mail addresses: machongyang@live.com (C. Ma), shirlyding@163.com (X. Wang), fafengcheng@gmail.com (F. Cheng).
[1] Tian Xu and Jiahui Chen contributed equally to this work.

https://doi.org/10.1016/j.heliyon.2024.e34718
Received 9 April 2024; Received in revised form 15 July 2024; Accepted 15 July 2024
Available online 20 July 2024

the population, rendering it a significant public health concern [1]. NAFLD represents a continuous spectrum of liver injuries, spanning from the accumulation of liver fat and triglycerides without specific symptoms to non-alcoholic steatohepatitis (NASH), covering multiple pathological processes such as inflammation, necrosis, apoptosis and fibrosis [2]. NASH is anticipated to emerge as a leading reason for liver transplantation in the coming decades [3]. Rezdiffra stands out as the sole drug to have recently received FDA approval, heralding it as the first-ever medication to be sanctioned for the treatment of NASH.

Traditional Chinese Medicine (TCM) presents a promising therapeutic avenue for addressing NASH [4]. Rooted in TCM theory, the primary pathological factor implicated in NASH involve in an excess of heat and fire toxins, coupled with the concurrent accumulation of blood stasis and phlegm evil. In response to these pathophysiological manifestations, a myriad of Chinese herbs and prescriptions have surfaced, with efficacy in heat clearance and detoxification [5], promotion of blood circulation and alleviation of blood stasis [6], as well as mitigation of phlegm and dampness [7]. Coptidis Rhizoma (Chinese name: Huang-Lian) and Bovis Calculus (Chinese name: Niu-Huang) examplify a classic herb pairing within TCM formulas, such as Angong Niuhuang pill and Niuhuang Jiedu pill, celebrated for their heat-clearing and detoxifying properties. Modern pharmacological research has revealed diverse pharmacodynmic properties associated with Coptidis Rhizoma, spanning anti-inflammation, anti-obesity, and anti-hepatic steatosis, and anti-metabolic diseases [8,9]. Berberine, a natural alkaloid derived from Coptidis Rhizoma, has demonstrated the capacity to reshape gut microbiome composition and ameliorate insulin resistance induced by high-fat diet (HFD) [10]. It is noteworthy that berberine has advanced to phase 4 clinical trials for the treatment of NASH [11]. In parallel, Bovis Calculus has garnered substantial attention due to its favorable effects, encompassing the inhibition of inflammatory responses, mitigation of oxidative stress, inhibition of apoptosis, and regulation of bile acid profiles [12]. Bovis Calculus has also been reported to reduce the levels of triglycerides, total cholesterol, and free fatty acids in fatty liver conditions [13]. Nonetheless, the biological basis of the anti-NASH action of the Coptidis Rhizoma- Bovis Calculus herb pair remains largely unexplored.

Drawing from the principles of multi-component, multi-target, and multi-pathway effects in TCM, network pharmacology has emerged as a valuable tool to explore the potential molecular basis and biological mechanisms underlying TCM interventions from a systematic perspective [14,15]. Therefore, in the current study, a network pharmacology strategy was used to predict the potential mechanisms of the herb pair against NASH. Additionally, we used two animal models to study the therapeutic effects and molecular mechanisms.

2. Materials and methods

2.1. Data collection

Gene related to NASH were collected from DisGeNET database by inputting the key word “non-alcoholic steatohepatitis” [16]. Bioactive compounds in the Coptidis Rhizoma and Bovis Calculus herb pair (HP) were collected from the Traditional Chinese Medicine Systems Pharmacology (TCMSP, http://lsp.nwu.edu.cn/index.php) database [17] and SymMap database (https://www.symmap.org/) [18]. For TCMSP database, only compounds with the parameters of oral bioavailability (OB)$\geq$30 % and drug-likeness (DL)$\geq$0.18 were considered as bioactive compounds. For SymMap database, only quality ingredients, blood ingredients and metabolic ingredients were collected for further target predicting. Both TCMSP and SymMap databases were used to obtain related targets of these bioactive compounds in the herb pair.

2.2. Network construction and enrichment analysis

Cytoscape software (Version 3.8) was used to build up a compound-NASH target network for further analysis. The ClusterProfiler package of R 3.5.0 software is adopted to conduct gene ontology (GO) functional annotation and Kyoto Encyclopedia of Genes and Genomes (KEGG) pathway enrichment [19]. The gene ontology (GO) annotation of these genes includes three different terms, following biological process (BP), molecular function (MF) and cellular component (CC). KEGG pathway enrichment analysis was visualized using the ggplot2 package. Adjust P value < 0.05 was set to be significant. A suite of KEGG mapping tools, KEGG Mapper, was used for specific pathway visualization [20].

2.3. Preparation of the herb pair

The Coptidis Rhizoma was purchased from Qiancao Herbal Pieces Co., Ltd., Beijing, China and in vitro cultured Calculus Bovis was purchased from Jianmin Dapeng Co., Ltd., Wuhan, China. The weight ratio of Coptidis Rhizoma and in vitro cultured Calculus Bovis was 50:1. In brief, 50 g of Coptidis Rhizoma were weighed and soaked in distilled water for 1 h, and heat the oven to a boil, then simmer for another 1.5 h. Two layers of 100-mesh filter bags were filtered while hot, and then the remaining Coptidis Rhizoma was continued to cook for 30 min, and filtered again. The liquid was combined and concentrated in a rotary evaporator under reduced pressure. And then the liquid was placed in a freeze-drying dish, and dried through a freeze-dryer, and finally 6.7516 g Coptidis Rhizoma lyophilized powder was obtained. In vitro cultured Calculus Bovis was mixed with the above lyophilized powder and kept refrigerated at -20 °C until use.

2.4. Animals

Eight-week-old specific pathogen free (SPF) male C57BL/6J mice (23 $\pm$ 2 g) were purchased from Sipeifu Laboratory Animal

Technology Co., LTD., Beijing, China. The feeding conditions were dark and light for 12 h, respectively. The temperature was controlled at 25 ± 1 °C, the humidity was controlled at 55 ± 10 % without noise interference (the background noise value was 40 ± 10 dB). The experimental design and procedures were approved and supervised by the Animal Ethics Committee of Beijing University of Chinese Medicine. Experimental ethical approval number: BUCHM-4-2022090902-3082.

2.5. High-fat diet (HFD) induced model

The fifty-four experimental mice were also divided into six groups, following control group (Chow), HFD group (HFD), low dose of herb pair group (HPL, 151.5 mg/kg of herb pair), middle dose of herb pair group (HPM, 303 mg/kg of herb pair), high dose of herb pair group (HPH, 606 mg/kg of herb pair) and Metformin group (Met, 200 m/kg). All animals began to model after one week of adaptive feeding and fed with control diet (D12450J, SYSE-Bio Co., Ltd., Changzhou, China) or High-fat diet (PD6001, SYSE-Bio Co., Ltd., Changzhou, China) for fourteen weeks. From the ninth week, drugs were given via intragastric administration while the control group and model group were given the same amount of saline.

2.6. Methionine-choline deficient diet (MCD) induced model

The forty-eight mice were randomly divided into six groups, following control group (Chow), MCD model group (MCD), low dose of herb pair group (HPL, 151.5 mg/kg of herb pair), middle dose of herb pair group (HPM, 303 mg/kg of herb pair), high dose of herb pair group (HPH, 606 mg/kg of herb pair) and Metformin (D9351, Solarbio, Beijing, China) group (Met, 200 m/kg). Mice were fed with standard methionine and choline-sufficient (MCS) diet (A2003B, SYSE-Bio Co., Ltd., Changzhou, China) or MCD diet (A2002B, SYSE-Bio Co., Ltd., Changzhou, China) for six weeks as previously published [21]. The treated groups were given different drug for the last four weeks via intragastric administration, while untreated groups were given saline solution. At the end of the experiment, mice were anesthetized with pentobarbital sodium, and the liver and serum were collected for further studies.

2.7. Oral glucose tolerance test (OGTT)

The OGTT was following previous detection methods with minor modifications [22]. Briefly, mice were fasted 12 h, and fasting blood glucose was measured. Then 20 % glucose (G8150, Solarbio Beijing, China) was administered by gavage immediately thereafter, blood glucose was recorded for 15, 30, 60, 90 and 120 min after glucose gavage administration.

2.8. Serum biochemistry analysis

Serum alanine aminotransferase (ALT), aspartate aminotransferase (AST), total bile acids (TBA), total cholesterol (TC), total triglycerides (TG), low density lipoprotein cholesterol (LDL-C) were detected by automatic biochemical analyzer (AU480, Beckman Coulter, USA).

2.9. Hematoxylin-eosin staining and oil red staining

After three days of liver tissue fixation, livers were then dehydrated with gradient ethanol, embedded in paraffin and sectioned. The hematoxylin-eosin (HE) staining (C0105 M, Beyotime, Shanghai, China) and Oil Red O staining (G1261, Solarbio, Beijing, China) were performed, and the pathological sections were observed using a light microscope (IX51, Olympus, Tokyo, Japan). and photographed for records [23].

2.10. RNA sequencing

Liver samples from mice in the Chow, HFD, and HPM groups (n = 3) were used for RNA sequencing experiment. Total RNA was extracted from the tissue using TRIzol® Reagent according the manufacturer's instructions. RNA purification, reverse transcription, library construction and sequencing were performed at Shanghai Majorbio Bio-pharm Biotechnology Co., Ltd. (Shanghai, China) according to the manufacturer's instructions (Illumina, San Diego, CA). The raw paired end reads were trimmed and quality controlled by fastp with default parameters. Then clean reads were separately aligned to reference genome with orientation mode using HISAT2 software. The mapped reads of each sample were assembled by StringTie in a reference-based approach.

To identify DEGs (differential expression genes) between two different samples, the expression level of each transcript was calculated according to the transcripts per million reads (TPM) method. RSEM was used to quantify gene abundances. Essentially, differential expression analysis was performed using the DESeq2. DEGs with $|\log2FC| \geq 1$ and p-value <0.05 were considered to be significantly different expressed genes. In addition, functional-enrichment analysis including GO and KEGG were performed to identify which DEGs were significantly enriched in GO terms and metabolic pathways at Bonferroni-corrected p-value <0.05 compared with the whole-transcriptome background. All data were analyzed on the online platform of Majorbio Cloud Platform (https://cloud.majorbio.com/).

2.11. Western blotting

Proteins were extracted from liver tissues by using RIPA lysis buffer(C1053, APPLYGEN, Beijing, China) containing protease inhibitor cocktail (P1265, APPLYGEN, Beijing, China) and PMSF (A1100, APPLYGEN, Beijing, China), and then the protein concentration was determined by BCA method (KGP902, KeyGEN, Nanjing, China). Proteins were separated by sodium dodecyl sulfate-polyacrylamide gel electrophoresis (SDS-PAGE) gels (PG112, Epizyme, Shanghai, China), and transferred to PVDF membranes (IPVH00010, Millipore, USA). The membrane was blocked with 5 % skim milk (P1622, APPLYGEN, Beijing, China) and then incubated with primary antibodies: NLRP3 (1:1000, ab263899, ABCAM, Cambridge, UK), IL-1 beta (1:1000, ab283818, ABCAM, Cambridge, UK), pro Caspase-1+p10+p12 (1:1000, ab179515, ABCAM, Cambridge, UK), ASC (1:1000, 67824S, CST, Massachusetts, USA), and β-actin (1:5000, 20536-1-AP, Proteintech, Chicago, USA). Then the membrane was incubated with HRP-conjµgated Affinipure Goat Anti-Rabbit IgG(H + L) (1:10000, SA00001-2, Proteintech, Chicago, USA). Finally, all blots were imaged with the aid of ECL chemiluminescence system (Tanon 5200, Shanghai, China).

2.12. Statistical analysis

Graphpad Prism 8.3.0 software was used to analyze the experimental data of this study. After normal distribution and homogeneity of variance test, the experimental data of each group were expressed as mean ± standard error of the mean ($\overline{x} \pm$ sem). One-way analysis of variance (ANOVA) with Bonferroni's test as post hoc test was used for analysis. $P < 0.05$ was considered as statistical difference.

3. Results

3.1. Network pharmacological analysis shows the herb pair modulates Nod-like receptor pathway

After an extensive screening of the TCMSP and SymMap databases, we identified 45 bioactive compounds from Coptidis Rhizoma and 10 bioactive compounds from Calculus Bovis. The Venny diagram analysis revealed 98 overlapping targets between the herb pair and NASH, which were recognized as potential targets of the herb pair against NASH (Fig. 1a). The network depicting the interactions between active compounds and NASH targets effectively demonstrated the multi-component and multi-target properties of this herb pair (Fig. 1b). GO enrichment analysis indicated that these overlapping targets were primarily associated with response to lipopolysaccharide, cytokine activity, and cytokine receptor binding. The top 10 BP, CC and MF terms were visually presented in Fig. 2a–c. In terms of KEGG enrichment analysis, the identified pathways mainly included the Toll-like receptor signaling pathway, Non-alcoholic fatty liver disease and the NOD-like receptor signaling pathway (Fig. 2d). Furthermore, using KEGG mapper, we constructed a schematic diagram illustrating how the herb pair modulates the NOD-like receptor pathway against NASH (Fig. 2e). In this diagram, yellow nodes represent targets related solely to the herb pair, red nodes indicate targets related to both herb pair and NASH,

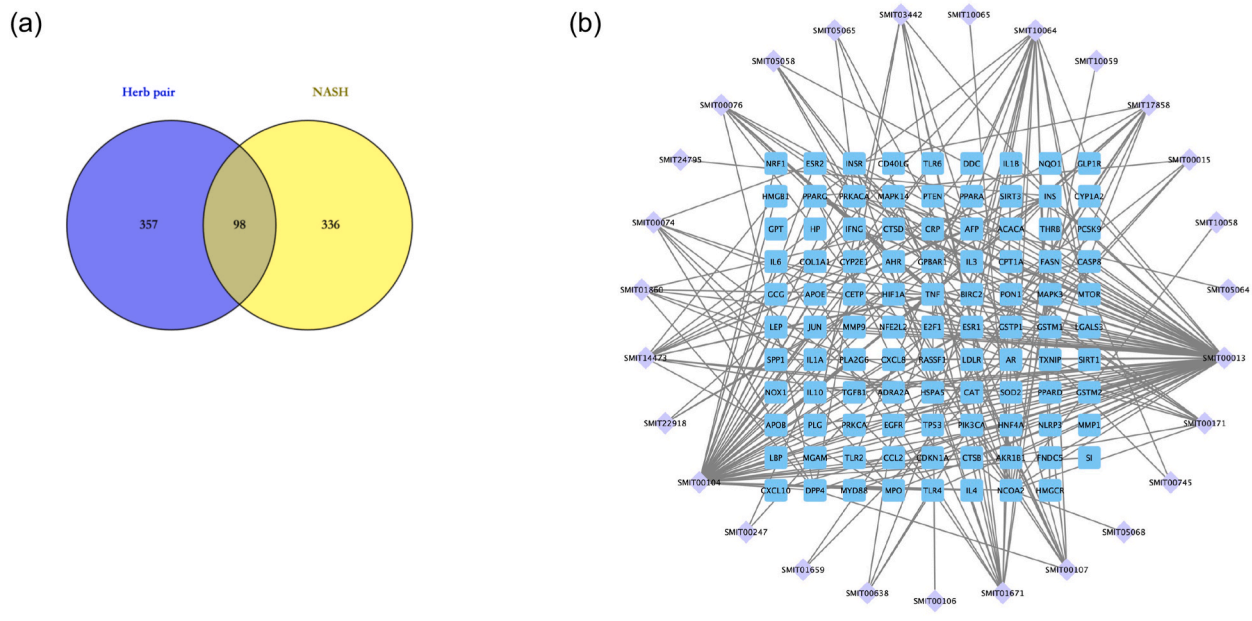

Fig. 1. Prediction of bioactive compounds and target in herb pair. (a) Venny diagram of herb pair targets and NASH genes. (b) A compound-target network of herb pair.

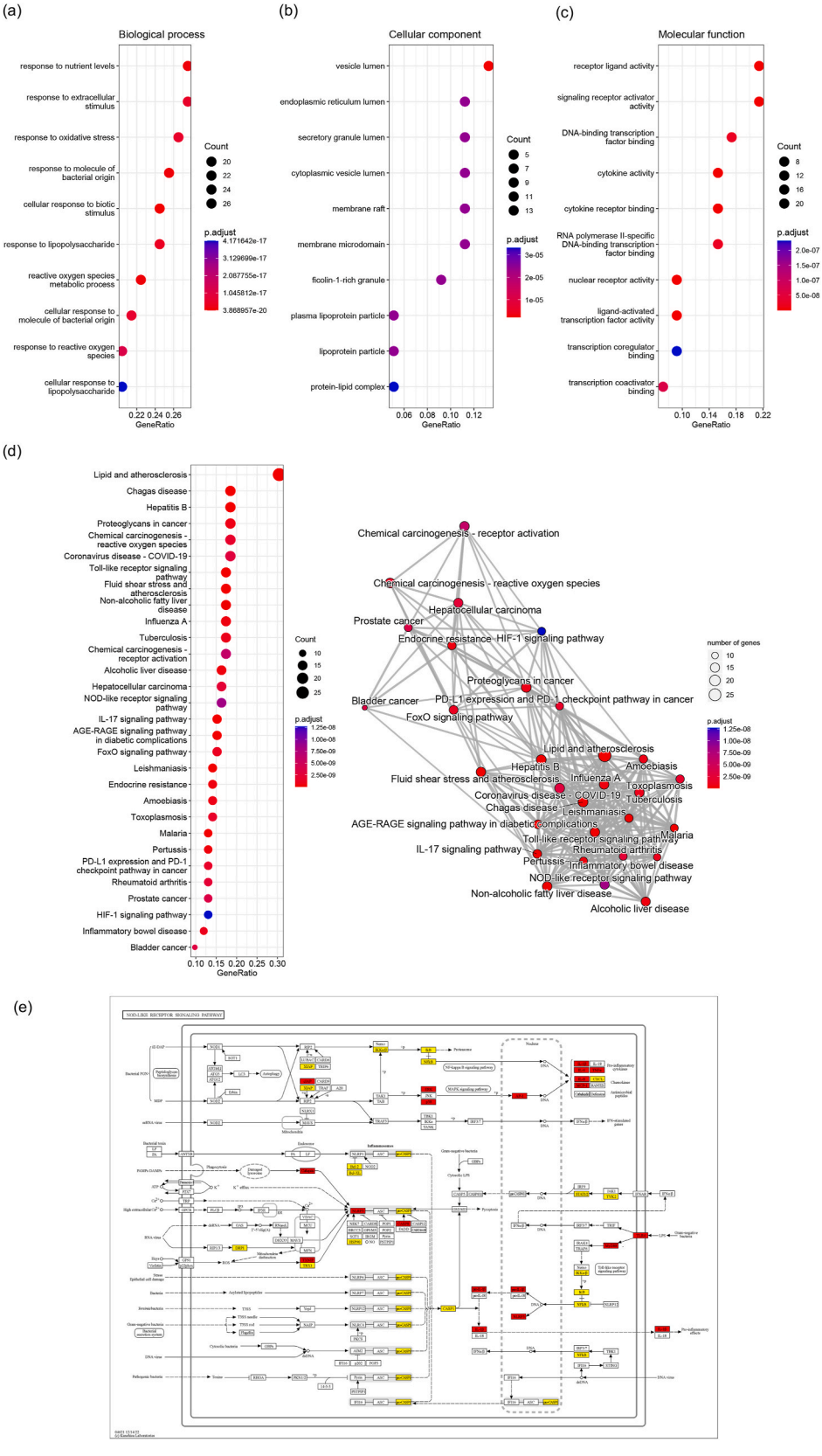

(caption on next page)

Fig. 2. Enrichment analysis of herb pair in the treatment of NASH. GO analysis including (a) Biological process. (b) Cellular component. (c) Molecular function. (d) KEGG enrichment analysis. (e) NOD-like receptor pathway schematic diagram.

and white nodes denote other proteins within the pathway.

3.2. Herb pair improves insulin sensitivity in HFD-induced NAFLD model

After 14-week experiment, the body weight of HFD-fed mice was significantly increased compared with Chow group, and intervention of herb pair or metformin significantly decreased body weight (Fig. 3a and b). Then, we investigated the impact of the herb pair on glucose tolerance in HFD-induced fatty liver mice, herb pair significantly decreased the AUC with a dose-dependent manner, and metformin treatment which was used a positive control also decreased AUC with significant difference (Fig. 3c and d).

3.3. Herb pair ameliorates HFD-induced liver injury

The serum biochemical analysis revealed that a high-fat diet (HFD) led to elevated levels of ALT, AST, TBA, TC, TG, and LDL-C. In all dosage groups of the herb pair, there was a notable and dose-dependent reduction in ALT and TBA levels compared to the HFD group (Fig. 4a and c). Only the high-dosage group demonstrated a significant reduction in serum AST and LDL-C levels when compared to the HFD group (Fig. 4b and f). Both the middle- and high-dosage groups exhibited a decrease in TC and TG levels when compared to the HFD group (Fig. 4d and e). Furthermore, in the Chow group, the liver exhibited a dark red color without noticeable enlargement, while in the HFD group, the liver was enlarged, displaying a dark yellow hue and greasy appearance. Following herb pair and metformin treatments, the liver exhibited an improved appearance compared to the HFD group (Fig. 4g). Histological examination of the liver revealed the absence of obvious lesions in the Chow group. However, HE staining indicated structural abnormalities and deformities in hepatocytes in the HFD group; Oil Red O staining demonstrated a significant increase in lipid droplet aggregation in the HFD group. Importantly, the herb pair and Met treatments alleviated all these observed phenomena (Fig. 4g).

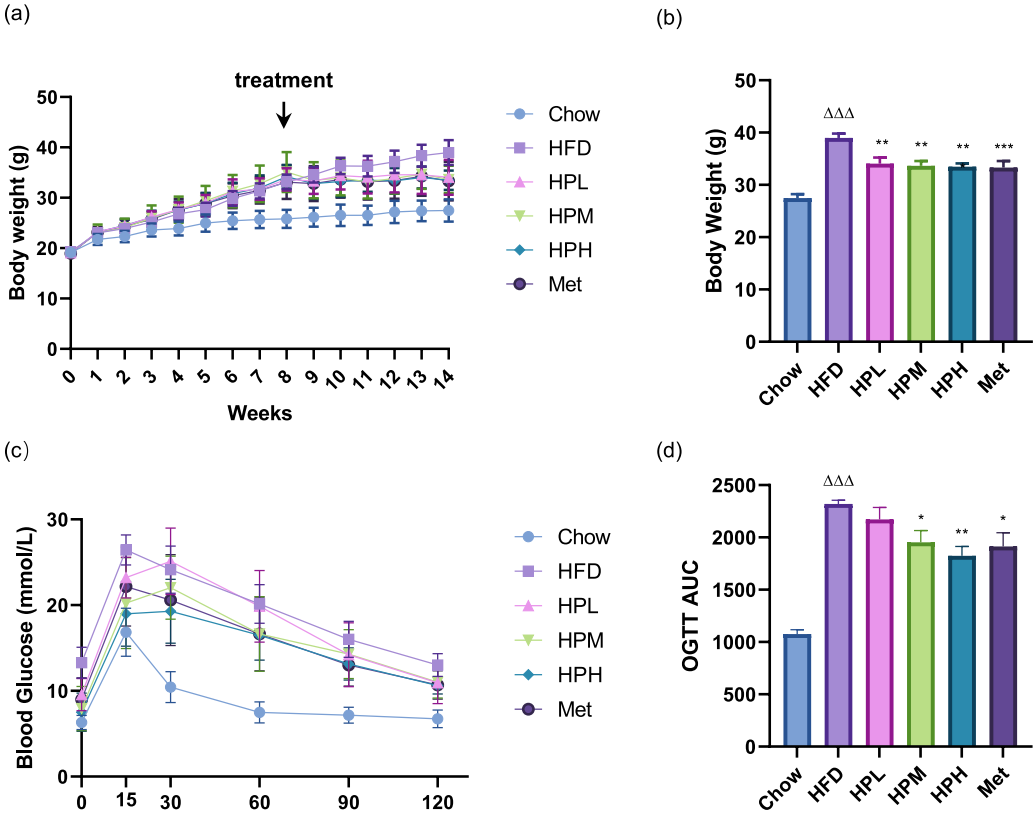

Fig. 3. Treatment with herb pair improves insulin sensitivity in HFD mice. (a) Changes in body weight during the modeling period. (b) Body weight after 14 weeks of modeling. (c) OGTT after 13 weeks of modeling. (d) AUC after 13 weeks of modeling. Compared with Chow: △△△$p < 0.001$; compared with HFD: *$p < 0.05$, **$p < 0.01$, ***$p < 0.001$.

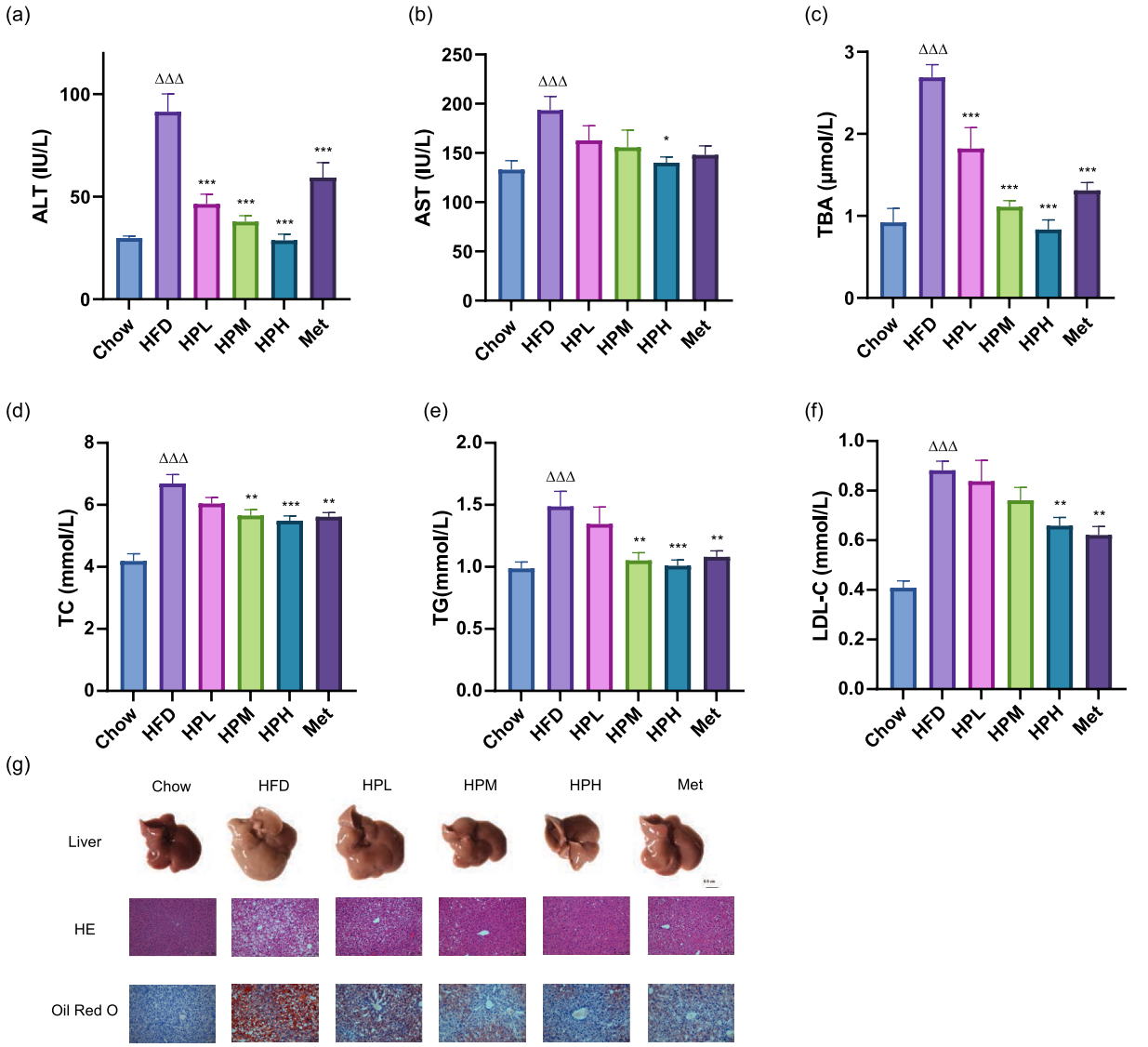

Fig. 4. Treatment with herb pair alleviates liver injury in HFD mice. (a) Serum ALT. (b) Serum AST. (c) Serum TBA. (d) Serum TC. (e)Serum TG. (f) Serum LDL-C. (g) Liver, H&E staining and Oil Red O staining of representative sections. Compared with Chow: △△△$p < 0.001$; compared with HFD: *$p < 0.05$, **$p < 0.01$, ***$p < 0.001$.

3.4. Herb pair inhibits the NLRP3 mediated NOD-like receptor pathway in HFD liver

We conducted RNA-Seq analysis to investigate the potential mechanisms responsible for the amelioration of NASH by the herb pair. This analysis revealed 1171 differentially expressed genes (DEGs) between the HFD and Chow groups and 1602 DEGs between the herb pair and HFD groups (Fig. 5a and b). Among these genes, 325 DEGs were found to be related to both the HFD and herb pair treatment, and we have represented their expression patterns in a heat-map (Fig. 5c and d). Moreover, the KEGG analysis highlighted that the overlapping DEGs were significantly enriched in the NOD-like receptor signaling pathway (Fig. 5e). The GO analysis revealed that these DEGs were enriched in various inflammation-related terms, including positive regulation of interleukin-6 production, positive regulation of interleukin-1 production, leukocyte migration, defense response to Gram-positive bacterium, and immune receptor activity (Fig. 5f–h). To further investigate these transcriptional changes, we conducted a gene set-enrichment analysis (GSEA). As anticipated, the results confirmed a significant upregulation of the NOD-like receptor signaling pathway in the HFD group when compared to the Chow group. Interestingly, this pathway was found to be significantly suppressed in response to treatment with herb pair (Fig. 5i and j). Western blotting experiments revealed that the middle and high dosages of the herb pair significantly reduced the relative expression levels of NLRP3, cleaved caspase-1 and cleaved IL-1β (Fig. 6a–c, 6e). There were no significant differences were observed in the expression levels of pro-caspase-1, pro- IL-1β and ASC (Fig. 6a, d, 6f-g). These findings provide valuable insights into a novel mechanism by which the Coptidis Rhizoma and Calculus Bovis herb pair treats NASH, involving the suppression of the NLRP3-

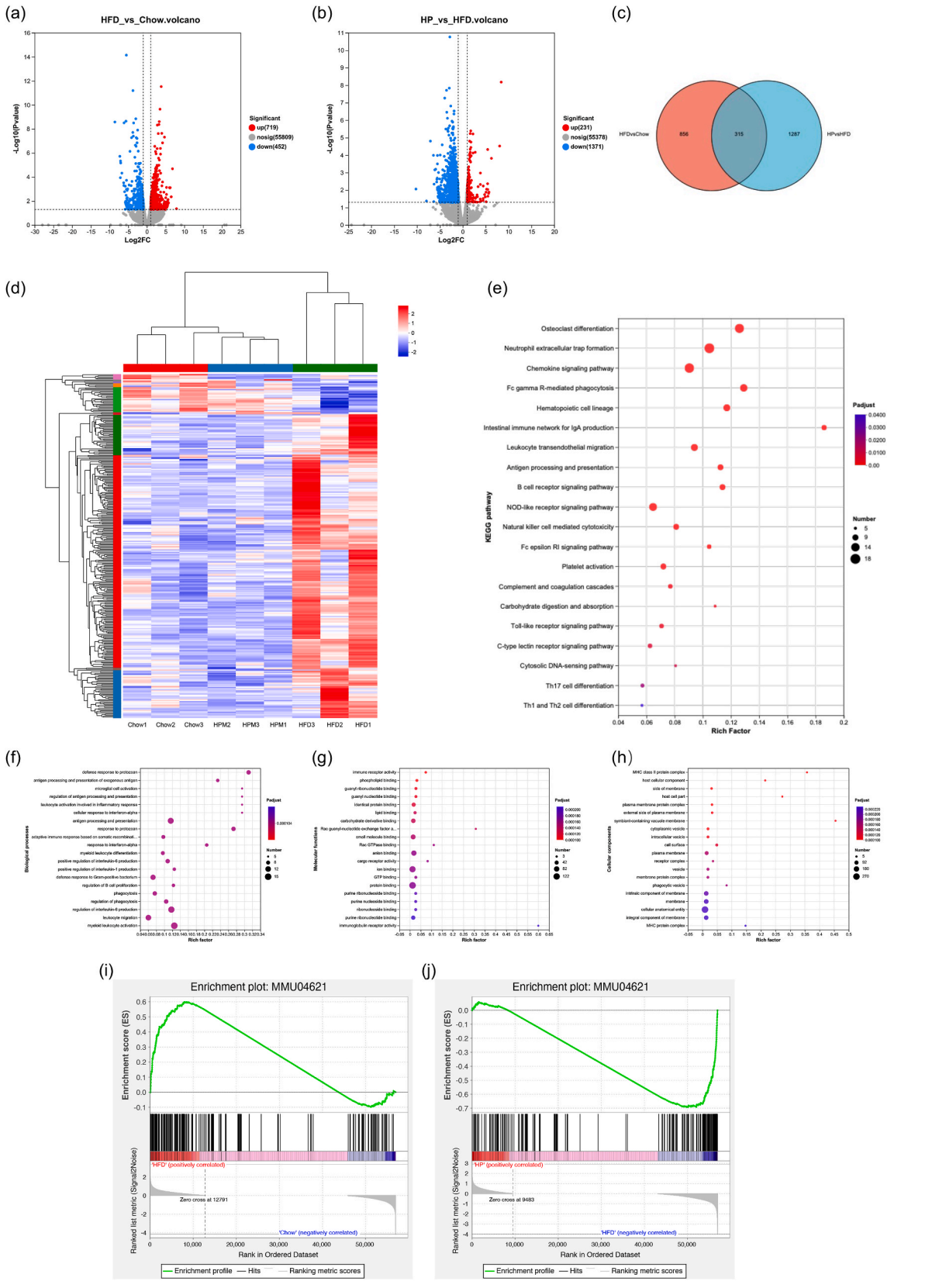

(caption on next page)

Fig. 5. Herb pair regulates the expression of inflammation-related genes in HFD mice. (a) Differentially expressed genes between HFD and Chow shown by Volcano Plot (log2FC≥|1| and adjust p-value <0.05). (b) Differentially expressed genes between herb pair and HFD shown by Volcano Plot (log2FC≥|1| and adjust p-value <0.05). (c) Differentially expressed genes related to both the HFD and herb pair treatment shown by venny diagram. (d) Differentially expressed genes related to both the HFD and herb pair treatment shown by heatmap. (e) KEGG pathway enrichment analysis of the significantly changed signaling pathways. GO analysis including (f) Biological process. (g) Cellular component. (h) Molecular function. (i) and (j) Gene set-enrichment analysis.

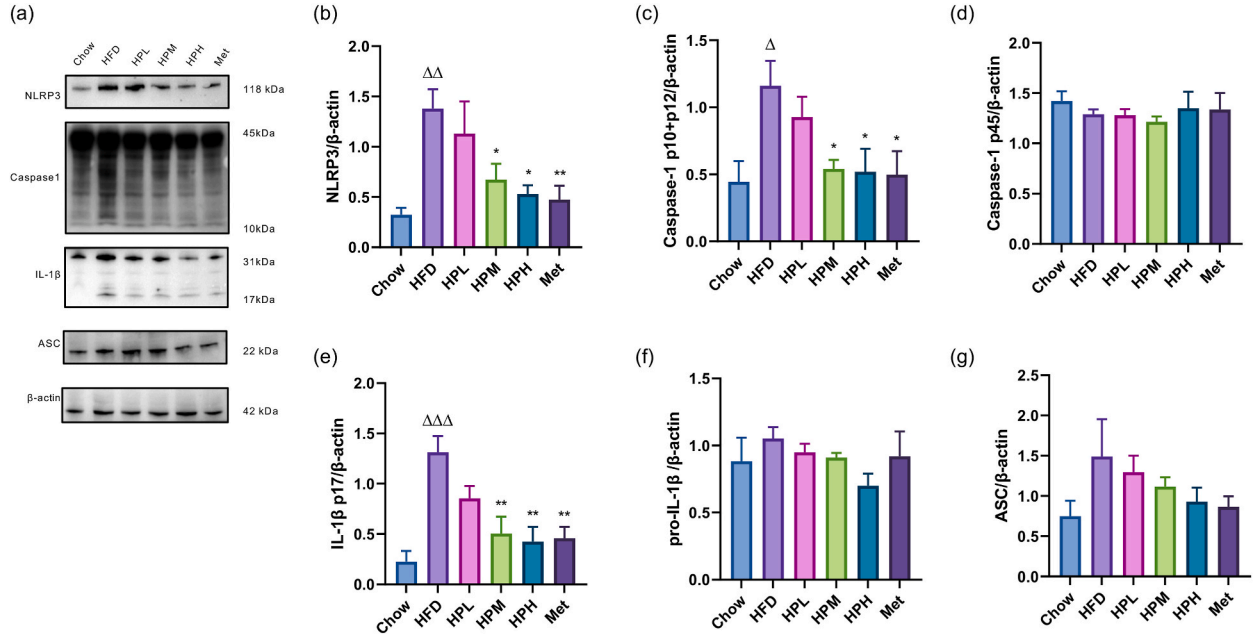

Fig. 6. Effects of herb pair alleviates NASH by inhibiting NLRP3 inflammasome in HFD mice. (a) The expression levels of NLRP3, Caspase-1, IL-1β, and ASC were analyzed by Western blotting. (b) Relative expression of NLRP3. (c) Relative expression of Caspase-1 p10+p12. (d) Relative expression of Caspase-1 p45. (e) Relative expression of IL-1β p17. (f) Relative expression of pro-IL-1β. (g) Relative expression of ASC. Compared with Chow: △p < 0.05, △△p < 0.01, △△△p < 0.001; compared with HFD: *p < 0.05, **p < 0.01.

mediated NOD-like receptor pathway.

3.5. Herb pair ameliorates MCD-induced liver injury

In order to investigate the modulating effect of the herb pair on the NLRP3 signal, we employed an alternative NASH model, specifically the MCD-induced NASH model. All the three dosages of the herb pair significantly reduced the levels of ALT and TBA compared to MCD group (Fig. 7a and c). Moreover, the middle and high dosages demonstrated a significant decrease in AST levels (Fig. 7b). Consistently, the overall liver morphology exhibited improvement, accompanied by a reduction in inflammation and lipid deposition within liver tissues after the herb pair treatment (Fig. 7d).

3.6. Herb pair inhibits the NLRP3 mediated NOD-like receptor pathway in MCD liver

In comparison to the Chow group, the liver of the MCD group exhibited significantly increased expression levels of NLRP3, cleaved Caspase-1, and cleaved IL-1β (Fig. 8a–c, 8e). This observation suggests the activation of the NLRP3 signaling pathway in the MCD-induced liver model. However, when compared to the MCD group, the liver samples from the middle and high dosages of the herb pair showed a significant decrease in the expression of NLRP3, cleaved Caspase-1, and cleaved IL-1β, indicating a noteworthy therapeutic effect. There were no observable changes in the expression levels of pro-caspase-1, pro-IL-1β, and ASC in the liver following treatment with the herb pair (Fig. 8a, d, 8f-g).

4. Discussion

The term "fatty liver" first appeared in the German literature in 1962 to describe fatty liver with necrotizing inflammation, its highlighted the similarities in histopathological findings but differences in clinical course between alcoholic and nonalcoholic causes of fatty liver [24]. However, the emergence of NASH as a technical term was first proposed by Ludwig and his colleagues at the Mayo

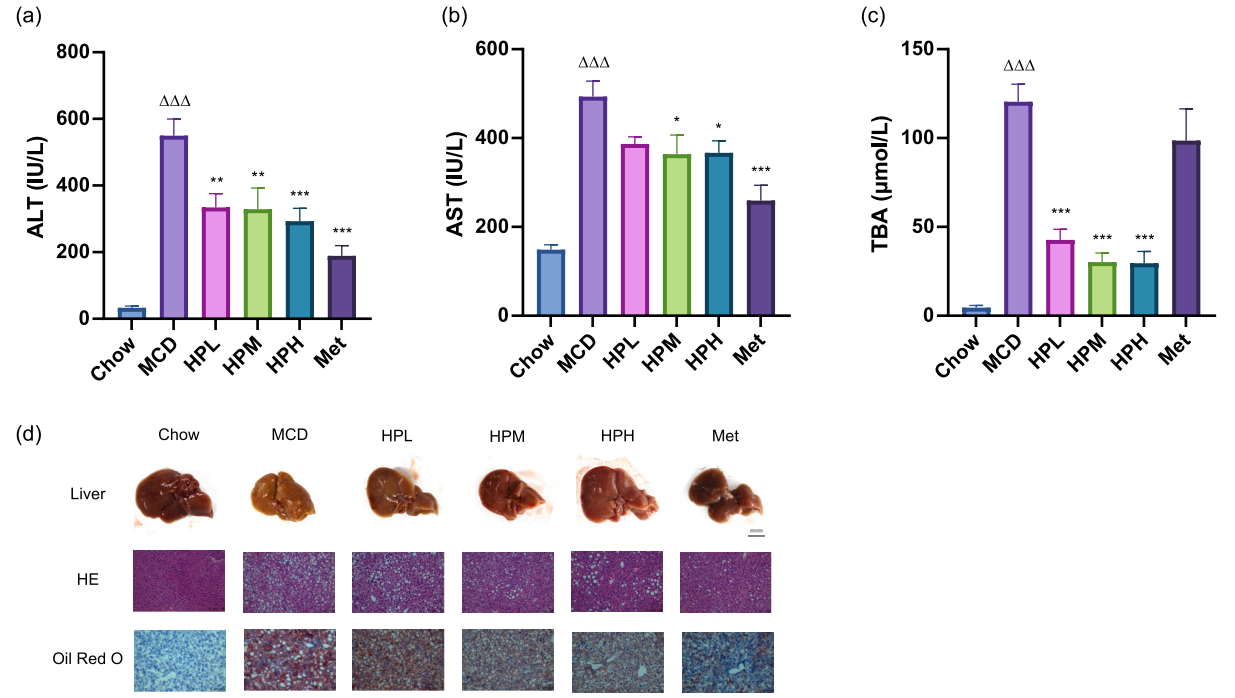

Fig. 7. Treatment with herb pair alleviates liver injury in MCD mice. (a) Serum ALT. (b) Serum AST. (c) Serum TBA. (d) Liver, H&E staining and Oil Red O staining of representative sections. Compared with Chow: △△△$p < 0.001$; compared with MCD: *$p < 0.05$, **$p < 0.01$, ***$p < 0.001$.

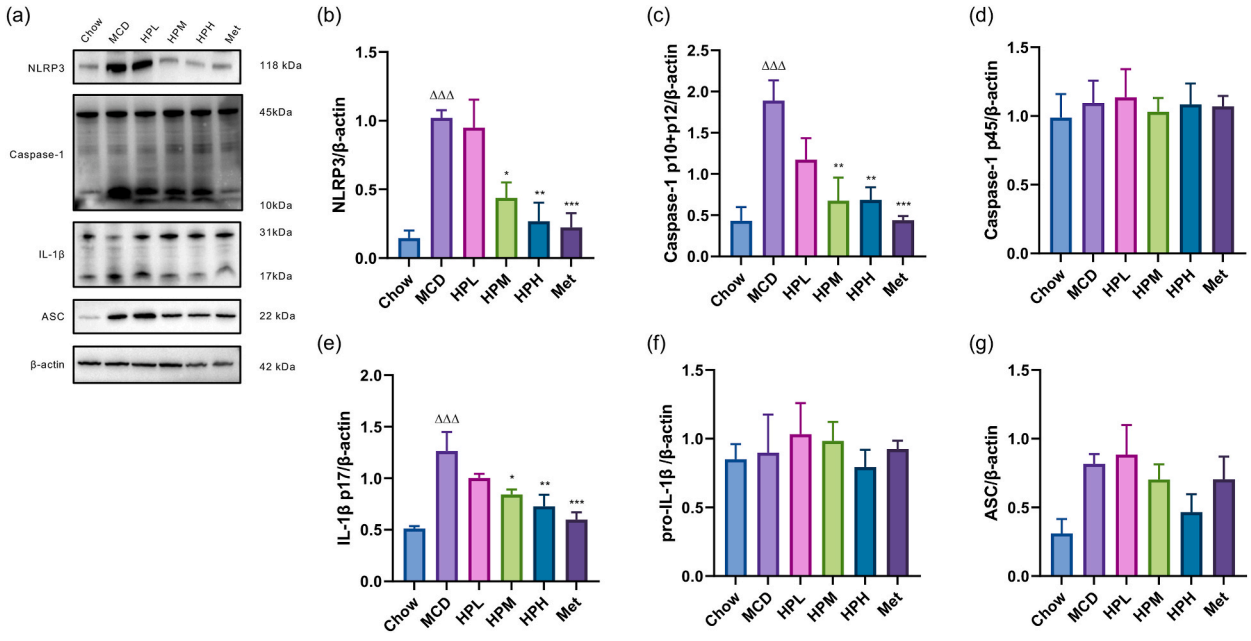

Fig. 8. Effects of herb pair alleviates NASH by inhibiting NLRP3 inflammasome in MCD mice. (a) The expression levels of NLRP3, Caspase-1, IL-1β, and ASC were analyzed by Western blotting. (b) Relative expression of NLRP3. (c) Relative expression of Caspase-1 p10+p12. (d) Relative expression of Caspase-1 p45. (e) Relative expression of IL-1β p17. (f) Relative expression of pro-IL-1β. (g) Relative expression of ASC. Compared with Chow: △△△$p < 0.001$; compared with MCD: *$p < 0.05$, **$p < 0.01$, ***$p < 0.001$.

Clinic in Rochester, Minnesota, in 1980. He defined it as "a hitherto unnamed liver disease, similar in histology to alcoholic hepatitis, which may also progress to cirrhosis" and represents a state of chronic inflammation of the liver [25]. The pathogenesis of NASH has experienced the traditional "second-hit" theory [26], the first hit is liver lipid accumulation caused by lipid metabolism disorders,

followed by liver inflammation and hepatocyte damage as the second hit. Now scholars put forward the "multiple hits" theory [27]: it involves the parallel regulation of genetic susceptibility, the regulation of complex metabolic pathways and multiple signaling pathways in the liver, the activation of intestinal flora, liver inflammatory cells, immune cells, vascular endothelial cells, and other specific content, which promotes the accumulation of liver fat and adipose tissue dysfunction, then induces the secretion of adipokines and inflammatory cytokines, which further confirms the complexity of this disease.

Liver excessive inflammation is one of the hallmarks features of NASH, and which is an important driving force for the progression of the disease, promoting persistent liver fibrosis, and eventually leading to cirrhosis [28]. Although the key mechanisms that lead to inflammation in patients with NASH are unknown, but several important contributing factors have been proposed. The initiation of inflammatory response is inseparable from inflammasome, among which NOD-like receptor thermal protein domain associated protein 3 (NLRP3) inflammasome is the most deeply studied [29]. As an intracellular multi-protein complex, the NLRP3 inflammasome can respond rapidly to exogenous and endogenous alarm signals [30]. The NLRP3 protein, ASC adaptor protein, and apoptosis-associated speck-like protein of Caspase-1 combine to form the NLRP3 inflammasome complex, which converts IL-1β and IL-18 into active forms, and induce NLRP3 inflammasome-related diseases [31]. Cholesterol levels are elevated in the liver of NASH and have been shown to be a lipotoxic Damage associated molecular patterns (DAMPs), it can induce the activate Kupffer cells and macrophages and release IL-1β [32]. Similar results were obtained in FFA-exposed Kupffer cells, which led to the activation of NLRP3 inflammasome and subsequent involvement in NASH-related Interleukin-1β (IL-1β) secretion [33]. Compared with NAFL patients, pro-IL-1β, pro-IL-18 and NLRP3 in liver biopsy of NASH patients were significantly increased [34]. This corresponds to data observed in NASH patients, where IL-1β levels are significantly increased compared to NAFLD and healthy individuals [35]. Another study also showed that NLRP3 inflammasome was activated in NASH patients, accompanied by caspase-1-dependent increase in IL-1β secretion [36]. Blockade of NLRP3 expression by NLRP3 inhibitors has been reported to be an effective treatment. Drugs targeting NLRP3 can improve liver function, reduced liver inflammation, inhibited the expression and activity of Caspase-1, and reduced the expression levels of pro-inflammatory cytokines such as IL-1β and IL-18 [37].

Considering the disease complexity and economic burden of NASH, as well as the lack of effective pharmacological interventions, there is an urgent need for in-depth research on the pathogenesis to develop more targeted and efficient treatment strategies. The clinical research of NASH is limited by many ethical factors, especially the collection of patients' tissue samples, moreover, as a chronic liver disease, the disease process of NASH may last for several years or even decades, which seriously limits the quality of clinical data [38]. Therefore, it is necessary to establish animal models to elucidate the physiological, pathological mechanisms, and therapeutic targets of NASH [39]. Due to its histological similarity to human NASH, MCD-induced steatohepatitis in rodents is the most classic animal model of NASH, and is often used to study the pathogenesis of NASH and the therapeutic effect of intervention drugs [40]. The MCD diet consists of 40 % sucrose and 10 % energy from lipids, but lacks methionine and choline [41]. Compared with other diet-induced NASH animal models, MCD-induced NASH animal models can cause weight loss [42], and the animals can develop a severe NASH phenotype in the shortest time (2–4 weeks) [43], seriously affect liver fat metabolism, it leads to the activation of inflammatory signals, endoplasmic reticulum stress, and lipid peroxidation [44], which transforms simple steatosis into steatohepatitis and finally induces obvious fibrotic lesions [45]. The effects of different doses of the herb pair on NASH mice model induced by MCD diet were evaluated. The study showed that the herb pair can reduced serum ALT, AST and TBA levels, also improved the general morphology and pathological manifestations of liver, and reduced the protein expression levels of NLRP3, cleaved Caspase-1 and cleaved IL-1β in the liver. Compared with the animal model of NASH induced by MCD diet, HFD can characterize the metabolic characteristics, oxidative stress and inflammatory response of obese NASH, but the liver damage is relatively mild, and will not reach the stage of liver fibrosis or cirrhosis. Besides, the liver function indexes of experimental animals can be restored after cessation of HFD intervention [46]. One of the most critical factors when adopting the HFD model is the need for prolonged feeding, usually greater than 10 weeks, to develop symptoms such as obesity, hepatic steatosis, and liver inflammation [47]. C57BL/6J mice were fed HFD for 14 weeks to prepare NASH mouse model, the herb pair also showed similar therapeutic effects on HFD mice, the study showed that the herb pair can reduced blood sugar, reduced serum ALT, AST, TBA, TC, TG and LDL-C contents, also improved the general morphology and pathological manifestations of liver, and reduced the protein expression levels of NLRP3, cleaved Caspase-1 and cleaved IL-1β in the liver. The current study found that regulation of NLRP3 inflammasome signaling pathway may be a key mechanism for the herb pair to improve NASH.

The current research has several limitations. Initially, the bioactive compounds were not subjected to evaluation through animal models, which would have provided a more comprehensive understanding of their effects. Additionally, the study's design confines its conclusions to demonstrating the herb pair's ability to prevent the activation of the NLRP3 pathway in a NASH model. It does not elucidate the specific upstream targets that may be involved. Consequently, it is imperative for future research to investigate and identify which bioactive compounds are capable of effectively inhibiting the NLRP3 pathway. This will contribute to a more targeted and efficacious approach to managing NASH.

5. Conclusion

This study has demonstrated the efficacy of the Coptidis Rhizoma and Calculus Bovis herb pair in alleviating NASH in various in vivo models. Both network pharmacology predictions and RNA-seq experiments have elucidated the potential mechanisms underlying the herb pair's action against NASH through the modulation of the NLRP3 signal. Notably, our experimental findings have provided direct evidence demonstrating the herb pair's efficacy in effectively inhibiting the activation of the NLRP3 signal, corroborating the analytical results.

Data availability statement

Data will be made available on request.

CRediT authorship contribution statement

Tian Xu: Writing – original draft, Validation, Methodology, Investigation, Conceptualization. **Jiahui Chen:** Validation, Methodology, Investigation, Conceptualization. **Qi Shao:** Writing – original draft, Methodology. **Jing Ji:** Investigation, Data curation. **Qingguo Wang:** Funding acquisition, Conceptualization. **Chongyang Ma:** Writing – review & editing, Funding acquisition. **Xueqian Wang:** Supervision, Conceptualization. **Fafeng Cheng:** Resources, Project administration.

Declaration of competing interest

The authors declare that they have no known competing financial interests or personal relationships that could have appeared to influence the work reported in this paper.

Acknowledgments

The study was funded by grants from the National Science Foundation of China (No. U21A20400, 82374165, 82004327).

Appendix A. Supplementary data

Supplementary data to this article can be found online at https://doi.org/10.1016/j.heliyon.2024.e34718.

References

[1] R.F. Schwabe, I. Tabas, U.B. Pajvani, Mechanisms of fibrosis development in nonalcoholic steatohepatitis, Gastroenterology 158 (7) (2020) 1913–1928.
[2] J.F. Dufour, et al., Current therapies and new developments in NASH, Gut 71 (10) (2022) 2123–2134.
[3] A.C. Sheka, et al., Nonalcoholic steatohepatitis: a review, JAMA 323 (12) (2020) 1175–1183.
[4] X. Chen, et al., Systematic analysis of randomised controlled trials of Chinese herb medicine for non-alcoholic steatohepatitis (NASH): implications for future drug development and trial design, Chin. Med. 18 (1) (2023) 58.
[5] L. Li, et al., Investigating pharmacological mechanisms of andrographolide on non-alcoholic steatohepatitis (NASH): a bioinformatics approach of network pharmacology, Chin Herb Med 13 (3) (2021) 342–350.
[6] S.M. Ren, et al., Systematic characterization of the metabolites of defatted walnut powder extract in vivo and screening of the mechanisms against NAFLD by UPLC-Q-Exactive Orbitrap MS combined with network pharmacology, J. Ethnopharmacol. 285 (2022) 114870.
[7] H. Ye, et al., Poria cocos polysaccharides rescue pyroptosis-driven gut vascular barrier disruption in order to alleviates non-alcoholic steatohepatitis, J. Ethnopharmacol. 296 (2022) 115457.
[8] J. Wang, et al., Coptidis Rhizoma: a comprehensive review of its traditional uses, botany, phytochemistry, pharmacology and toxicology, Pharm. Biol. 57 (1) (2019) 193–225.
[9] L. He, et al., Current advances in Coptidis rhizoma for gastrointestinal and other cancers, Front. Pharmacol. 12 (2021) 775084.
[10] X. Zhang, et al., Structural changes of gut microbiota during berberine-mediated prevention of obesity and insulin resistance in high-fat diet-fed rats, PLoS One 7 (8) (2012) e42529.
[11] T. Yan, et al., Herbal drug discovery for the treatment of nonalcoholic fatty liver disease, Acta Pharm. Sin. B 10 (1) (2020) 3–18.
[12] D. Xiang, et al., Calculus Bovis Sativus alleviates estrogen cholestasis-induced gut and liver injury in rats by regulating inflammation, oxidative stress, apoptosis, and bile acid profiles, J. Ethnopharmacol. 302 (Pt A) (2023) 115854.
[13] W. He, et al., Hepatoprotective effect of calculus bovis sativus on nonalcoholic fatty liver disease in mice by inhibiting oxidative stress and apoptosis of hepatocytes, Drug Des Devel Ther 11 (2017) 3449–3460.
[14] C. Nogales, et al., Network pharmacology: curing causal mechanisms instead of treating symptoms, Trends Pharmacol. Sci. 43 (2) (2022) 136–150.
[15] F. Noor, et al., Network pharmacology approach for medicinal plants: review and assessment, Pharmaceuticals 15 (5) (2022).
[16] J. Piñero, et al., The DisGeNET knowledge platform for disease genomics: 2019 update, Nucleic Acids Res. 48 (D1) (2020) D845–d855.
[17] J. Ru, et al., TCMSP: a database of systems pharmacology for drug discovery from herbal medicines, J Cheminform 6 (2014) 13.
[18] Y. Wu, et al., SymMap: an integrative database of traditional Chinese medicine enhanced by symptom mapping, Nucleic Acids Res. 47 (D1) (2019) D1110–d1117.
[19] T. Wu, et al., clusterProfiler 4.0: a universal enrichment tool for interpreting omics data, Innovation 2 (3) (2021) 100141.
[20] M. Kanehisa, et al., KEGG for taxonomy-based analysis of pathways and genomes, Nucleic Acids Res. 51 (D1) (2023) D587–d592.
[21] J. Jian, et al., Rifaximin ameliorates non-alcoholic steatohepatitis in mice through regulating gut microbiome-related bile acids, Front. Pharmacol. 13 (2022) 841132.
[22] N. Hu, et al., Comparative evaluation of the effect of metformin and insulin on gut microbiota and metabolome profiles of type 2 diabetic rats induced by the combination of streptozotocin and high-fat diet, Front. Pharmacol. 12 (2021) 794103.
[23] T. Lan, et al., Cordycepin ameliorates nonalcoholic steatohepatitis by activation of the AMP-activated protein kinase signaling pathway, Hepatology 74 (2) (2021) 686–703.
[24] H. Thaler, [Fatty liver, its causes and concomitant diseases], Dtsch. Med. Wochenschr. 87 (1962) 1049–1055.
[25] J. Ludwig, et al., Nonalcoholic steatohepatitis: Mayo Clinic experiences with a hitherto unnamed disease, Mayo Clin. Proc. 55 (7) (1980) 434–438.
[26] C. Peng, et al., Non-alcoholic steatohepatitis: a review of its mechanism, models and medical treatments, Front. Pharmacol. 11 (2020) 603926.
[27] R. Loomba, S.L. Friedman, G.I. Shulman, Mechanisms and disease consequences of nonalcoholic fatty liver disease, Cell 184 (10) (2021) 2537–2564.
[28] S. Torres, et al., Mitochondria and the NLRP3 inflammasome in alcoholic and nonalcoholic steatohepatitis, Cells 11 (9) (2022).
[29] J. Fu, H. Wu, Structural mechanisms of NLRP3 inflammasome assembly and activation, Annu. Rev. Immunol. 41 (2023) 301–316.
[30] Y. Huang, W. Xu, R. Zhou, NLRP3 inflammasome activation and cell death, Cell. Mol. Immunol. 18 (9) (2021) 2114–2127.

[31] S. Paik, et al., An update on the regulatory mechanisms of NLRP3 inflammasome activation, Cell. Mol. Immunol. 18 (5) (2021) 1141–1160.
[32] A.R. Mridha, et al., NLRP3 inflammasome blockade reduces liver inflammation and fibrosis in experimental NASH in mice, J. Hepatol. 66 (5) (2017) 1037–1046.
[33] J. Pan, et al., Fatty acid activates NLRP3 inflammasomes in mouse Kupffer cells through mitochondrial DNA release, Cell. Immunol. 332 (2018) 111–120.
[34] A. Wree, et al., NLRP3 inflammasome activation is required for fibrosis development in NAFLD, J. Mol. Med. (Berl.) 92 (10) (2014) 1069–1082.
[35] K. He, et al., Inhibition of NLRP3 inflammasome by thioredoxin-interacting protein in mouse Kupffer cells as a regulatory mechanism for non-alcoholic fatty liver disease development, Oncotarget 8 (23) (2017) 37657–37672.
[36] T. Csak, et al., Fatty acid and endotoxin activate inflammasomes in mouse hepatocytes that release danger signals to stimulate immune cells, Hepatology 54 (1) (2011) 133–144.
[37] S. Torres, et al., The specific NLRP3 antagonist IFM-514 decreases fibrosis and inflammation in experimental murine non-alcoholic steatohepatitis, Front. Mol. Biosci. 8 (2021) 715765.
[38] F. Zhong, et al., Rodent models of nonalcoholic fatty liver disease, Digestion 101 (5) (2020) 522–535.
[39] S. Gallage, et al., A researcher's guide to preclinical mouse NASH models, Nat. Metab. 4 (12) (2022) 1632–1649.
[40] B. Zhu, et al., Indole supplementation ameliorates MCD-induced NASH in mice, J. Nutr. Biochem. 107 (2022) 109041.
[41] L. Sámano-Hernández, et al., Beneficial and deleterious effects of sitagliptin on a methionine/choline-deficient diet-induced steatohepatitis in rats, Biochimie 181 (2021) 240–248.
[42] K. Ning, et al., Epigallocatechin gallate protects mice against methionine-choline-deficient-diet-induced nonalcoholic steatohepatitis by improving gut microbiota to attenuate hepatic injury and regulate metabolism, ACS Omega 5 (33) (2020) 20800–20809.
[43] M. Vesković, et al., Effect of betaine supplementation on liver tissue and ultrastructural changes in methionine-choline-deficient diet-induced NAFLD, Microsc. Microanal. 26 (5) (2020) 997–1006.
[44] Y.A. Jung, et al., Sitagliptin attenuates methionine/choline-deficient diet-induced steatohepatitis, Diabetes Res. Clin. Pract. 105 (1) (2014) 47–57.
[45] Y.J. Heo, et al., Visfatin exacerbates hepatic inflammation and fibrosis in a methionine-choline-deficient diet mouse model, J. Gastroenterol. Hepatol. 36 (9) (2021) 2592–2600.
[46] H. Itagaki, et al., Morphological and functional characterization of non-alcoholic fatty liver disease induced by a methionine-choline-deficient diet in C57BL/6 mice, Int. J. Clin. Exp. Pathol. 6 (12) (2013) 2683–2696.
[47] E.S. Lee, et al., Curcumin analog CUR5-8 ameliorates nonalcoholic fatty liver disease in mice with high-fat diet-induced obesity, Metabolism 103 (2020) 154015.